ARTICLE

HemaSphere ⬡ eha

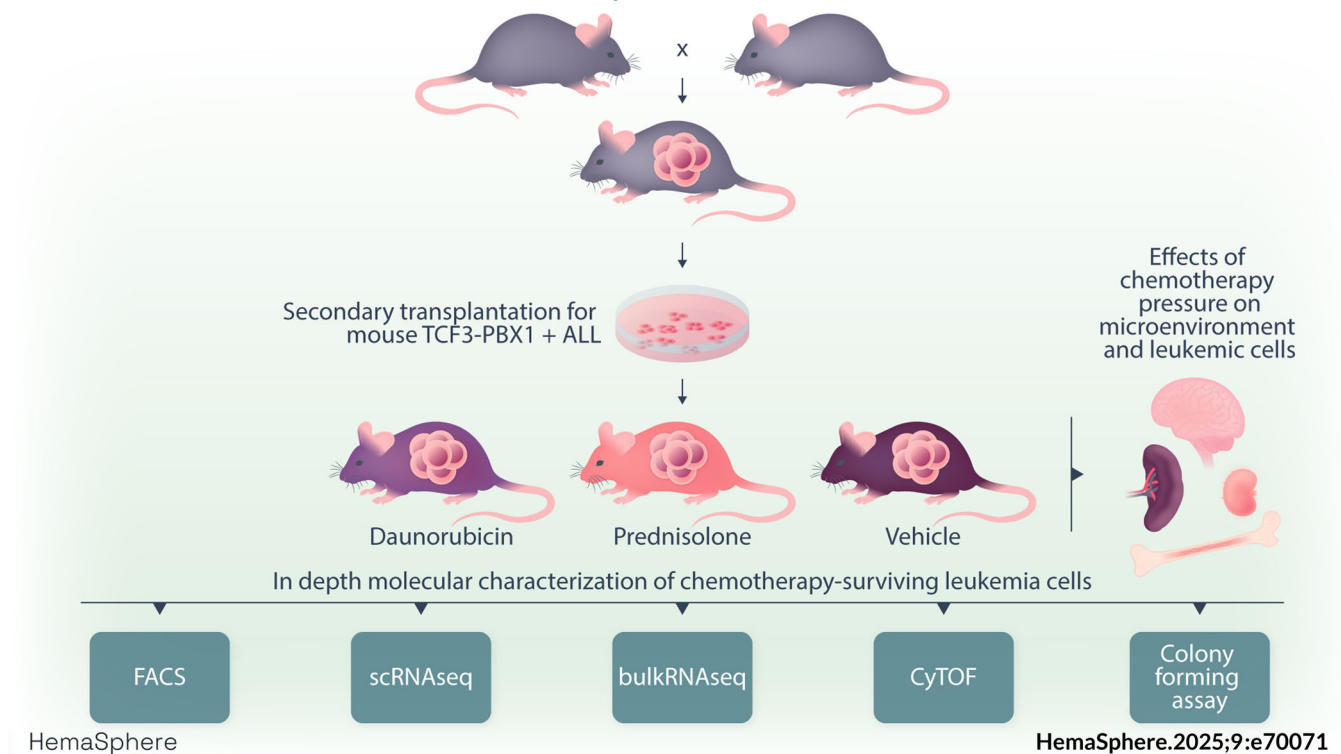# Dynamic evolution of TCF3-PBX1 leukemias at the single-cell level under chemotherapy pressure

Mira Kusterer[1,^] | Mari Lahnalampi[2,^] | Minna Voutilainen[2,^] |
Alexandra Brand[1,^] | Sandra Pennisi[1] | Johana Norona[1] | Gaia Gentile[1] |
Heike Herzog[1] | Gabriele Greve[1,3] | Michael Lübbert[1] | Mikko Sipola[2] |
Emma Kaartinen[2] 🆔 | Roman Sankowski[4] | Marco Prinz[4,5,6] | Saskia Killmer[7] |
Marilyn S. Lago[7] | Bertram Bengsch[5,7] | Stepan R. Cysar[8] | Konrad Aumann[8] |
Martin Werner[8] | Justus Duyster[1] | Olli Lohi[9] | Merja Heinäniemi[2,^] |
Jesús Duque-Afonso[1,^] 🆔

Graphical Abstract

HemaSphere ⬡ eha

Dynamic evolution of TCF3-PBX1 leukemias at the single-cell level under chemotherapy pressure

Mira Kusterer[1,^] | Mari Lahnalampi[2,^] | Minna Voutilainen[2,^] | Alexandra Brand[1,^] | Sandra Pennisi[1] | Johana Norona[1] | Gaia Gentile[1] | Heike Herzog[1] | Gabriele Greve[1,3] | Michael Lübbert[1] | Mikko Sipola[2] | Emma Kaartinen[2] | Roman Sankowski[4] | Marco Prinz[4,5,6] | Saskia Killmer[7] | Marilyn S. Lago[7] | Bertram Bengsch[5,7] | Stepan R. Cysar[8] | Konrad Aumann[8] | Martin Werner[8] | Justus Duyster[1] | Olli Lohi[9] | Merja Heinäniemi[2,^] | Jesús Duque-Afonso[1,^]

Correspondence: Merja Heinäniemi (merja.heinaniemi@uef.fi) and Jesús Duque-Afonso (jesus.duque.afonso@uniklinik-freiburg.de)

Abstract

Acute lymphoblastic leukemia (ALL) is the most common childhood cancer. The translocation t(1;19), encoding the TCF3-PBX1 fusion, is associated with intermediate risk and central nervous system (CNS) infiltration at relapse. Using our previously generated TCF3-PBX1 conditional knock-in mice, we established a model to study relapsed clones after in vivo chemotherapy treatment, CNS infiltration, and clonal dynamic evolution of phenotypic diversity at the single cell-level using next-generation sequencing technologies and mass cytometry. Mice transplanted with TCF3-PBX1+ leukemia cells and treated with vehicle succumbed to disease, whereas 40% of treated mice with prednisolone or daunorubicin survived. Bulk and single-cell RNA sequencing of FACS-sorted GFP+ cells from TCF3-PBX1+ leukemias arising after chemotherapy treatment revealed that apoptosis, interleukin-, and TGFβ-signaling pathways were regulated in CNS-infiltrating leukemic cells. Across tissues, upregulation of the MYC signaling pathway was detected in persisting leukemic cells and its downregulation by BRD3/4 inhibition increased sensitivity to chemotherapy. In TCF3-PBX1+ leukemia cells collected after chemotherapy treatment, mass cytometry identified increased phosphorylation of STAT3/5 upon preBCR stimulation, which was susceptible to inhibition by the proteasome inhibitor bortezomib. In summary, we developed a TCF3-PBX1+ ALL mouse model and characterized relapsed disease after in vivo chemotherapy and cell phenotype dependence on microenvironment. Transcriptomics and phospho-proteomics revealed distinct pathways that may underlie chemotherapy resistance and might be suitable for pharmacological interventions in human ALL.

[1]Department of Hematology, Oncology, Stem Cell Transplantation, Faculty of Medicine, University of Freiburg Medical Center, Freiburg, Germany

[2]Institute of Biomedicine, School of Medicine, University of Eastern Finland, Kuopio, Finland

[3]Institute of Genetic Epidemiology, Faculty of Medicine, University of Freiburg Medical Center, Freiburg, Germany

[4]Department of Neuropathology, Faculty of Medicine, University of Freiburg Medical Center, Freiburg, Germany

[5]Center for NeuroModulation, Faculty of Medicine, University of Freiburg, Freiburg, Germany

[6]Signaling Research Centers BIOSS and CIBSS, University of Freiburg, Freiburg, Germany

[7]Department of Gastroenterology, Hepatology, Endocrinology, and Infectious Disease, Faculty of Medicine, University of Freiburg Medical Center, Freiburg, Germany

[8]Department of Pathology, Faculty of Medicine, University of Freiburg Medical Center, Freiburg, Germany

[9]Tampere Center for Child, Adolescent, and Maternal Health Research, Faculty of Medicine and Health Technology, Tampere University, and Tays Cancer Centre Tampere University Hospital Tampere, Tampere, Finland

^Mira Kusterer, Mari Lahnalampi, Minna Voutilainen, Alexandra Brand are co-first authors and contributed equally. Merja Heinäniemi and Jesús Duque-Afonso are senior authors and contributed equally.

INTRODUCTION

Acute lymphoblastic leukemia (ALL) is the most common form of childhood cancer. The prognosis of children with ALL has improved during the last decades,[1] mainly through more intensive chemotherapy and radiotherapy treatments and risk stratification for high-risk patients.[2] Moreover, the development of novel therapies, including antibodies such as blinatumomab[3] or inotuzumab-ozogamicin[4] and cellular-based therapies as CAR-T cells[5] has improved the survival of patients with relapsed/refractory disease. While research has been focused on high-risk and relapsed/refractory patients, the biology of low-to-intermediate-risk patients has so far been inadequately investigated and can lead to overtreatment with severe side effects and/or undertreatment with risk of relapse.

The translocation t(1;19) codes for the chimeric fusion protein TCF3-PBX1 (also known as E2A-PBX1) formed by two key transcription factors (TFs) for lymphoid and embryonic development. Based on cytogenetic analysis in different cohorts, this subtype is associated with intermediate risk ALL.[6,7] However, it has been reported that TCF3-PBX1+ leukemias are associated frequently with central nervous system (CNS) relapse,[8,9] suggesting that TCF3-PBX1+ leukemias have specific properties for homing and/or survival in CNS niche under chemotherapy pressure.

To study the molecular pathogenesis and translational biology of TCF3-PBX1+ leukemias, we developed a TCF3-PBX1+ conditional knock-in mouse model. This preclinical model shares several genetic and clinical characteristics with TCF3-PBX1+ patients, including CNS infiltration of leukemic blasts.[10] Hence, the TCF3-PBX1+ conditional mice have been successfully used to study mechanisms of resistance to targeted therapies in preBCR+ ALL.[11] TCF3-PBX1+ leukemias are often associated with positivity for pre-B cell receptor (preBCR) signaling, involving expression of the subunits encoded by *Cd79a/b* genes. Overexpression of these signaling factors is increased in CNS-positive cases and correlates with time to relapse.[12,13] Further characterization of such changes in gene expression and signaling protein activity upon drug therapies is therefore of utmost importance to discover drug-targetable pathways that can counteract disease recurrence.

Mechanisms of chemotherapy resistance in ALL have been investigated by bulk gene-expression microarrays in the past.[14] Novel technologies based on next-generation sequencing technologies as whole-genome sequencing,[15] whole-exome sequencing,[16,17] and RNA sequencing (RNAseq)[18,19] have increased our knowledge about molecular pathogenesis of ALL. Recently, single-cell-based methods such as single-cell RNA sequencing (scRNAseq)[20] and mass cytometry (CYTOF)[21] have increased the resolution of transcriptome and antibody-based phenotypic cell-state identification and enabled their characterization even in the more challenging clinical context during drug treatment.[22]

Here, we established a model to study surviving leukemic cells after in vivo chemotherapy based on the conditional TCF3-PBX1+ knock-in mouse model. Based on genomic and protein profiles collected in bulk and at single-cell resolution, we show that our model recapitulates diversity of leukemic phenotypes enabling the characterization of critical microenvironmental, transcriptional, genomic, and signaling pathway activity adaptations of leukemic cells such as Myc signaling pathway upregulation and increase in phosphorylated STAT3/STAT5 levels after preBCR stimulation in cells exposed to chemotherapy. Overall, the dynamic changes of TCF3-PBX1+ leukemia cells under chemotherapy pressure were concordant between different tissues and under treatment with conventional chemotherapies such as prednisolone and daunorubicin and pave the way for the development of targeted therapies to overcome conventional chemotherapy resistance in human ALL.

MATERIALS AND METHODS

Secondary bone marrow transplantation assays

To develop a murine model to study relapsed ALL clones after chemotherapy treatment across tissues, recipient immunocompetent 8- to 12-week-old C57/BL6 healthy female mice (Janvier Labs) were sublethally irradiated (4.5–6 Gy) and transplanted intravenously via tail vein with 1000 mouse preBCR+/TCF3-PBX1+ GFP+ leukemia cells (M159[10]). After engraftment, 7 days after transplantation, mice were treated with vehicle intraperitoneally (dimethyl sulfoxide [DMSO] 2%, PEG300 30%, 2% Tween 80/d, n = 15), prednisolone intraperitoneally (20 mg/kg b.w./d, n = 15) or daunorubicin intraperitoneally (0.25 mg/kg b.w./d, n = 15) for 20 days. Mice were monitored for signs of disease 2–3 times per week and circulating GFP+ TCF3-PBX1+ leukemia cells were assessed by flow cytometry approximately every month. When end point criteria were reached, mice were euthanized and their organs were analyzed. Mice that died of toxicity of the treatment or without leukemia cells (vehicle = 2, prednisolone = 4, daunorubicin = 1) were excluded from final analysis but described in figure legends. No randomization method was used to allocate the animals to an experimental group. The investigators were not blinded to the group allocation during the experiment. Sample size was not calculated for mouse transplantation experiments. All experiments were performed in accordance with relevant guidelines and regulations and were approved by the "Regierungspräsidium Freiburg" (no. G19/179).

Histological staining

Leukemia cells in sacrificed mice were confirmed cytologically with May-Grünwald Giemsa staining of blood smears. Bone marrow (BM), liver, spleen (SP), lymph nodes (LN), brain, and spinal cord (SC) were isolated from euthanized mice, fixed in formalin 4%, and embedded in paraffin. 5 μm tissue sections were stained with hematoxylin-eosin with a standard protocol.

Bulk RNA sequencing

To compare the gene expression profiles of leukemic cells across tissues, RNA from BM, SP, LN, and CNS (brain and SC) was isolated using the RNeasy Plus Micro Kit (Qiagen) according to the manufacturer's instructions. RNA was used for RNAseq analysis following library preparation using the Illumina Stranded Total RNA Prep, Ligation with Ribo-Zero Plus kit. Sequencing was performed in the Max-Planck-Institute for Immunbiology and Epigenetics, Freiburg, Germany, using NovaSeq. 6000. Sequencing data were processed using nf-core/rnaseq pipeline (version 3.8). RNA quality was assessed by FastQC. MultiQC Reads were first trimmed to remove adapter sequences and poor-quality reads were removed with TrimGalore. Filtered-in reads were then aligned to the mouse genome (mm10) and read counts per gene were quantified using Salmon and post-processed with SAMtools and picard MarkDuplicates. The differential gene expression analysis was performed with the limma + voom pipeline (v. 3.16).

Single-cell RNA sequencing

Cells were fixed with methanol according to 10× Genomics Methanol Fixation of Cells for sc-RNA Sequencing protocol User guide CG000136 RevE. Cell suspension included mouse and human cells (unrelated study providing technical control for doublet rate) that were processed according to user guide CG000183 RevC of 10× Chromium

Single Cell 3′ GEM, Library and Gel Bead Kit v3. Sequencing was performed at Novogene UK sequencing core facility aiming at 50,000 reads per cell depth. Data processing was performed using Cellranger and R packages Seurat, scDD and SCEVAN, as described in Supporting Information Methods.

Pathway analysis with Enrichr

To study changes in gene expression more broadly than the level of specific individual genes, pathway analysis was performed. Enrichr[23] web-based tool was used, including 102 gene-set libraries. Pathway
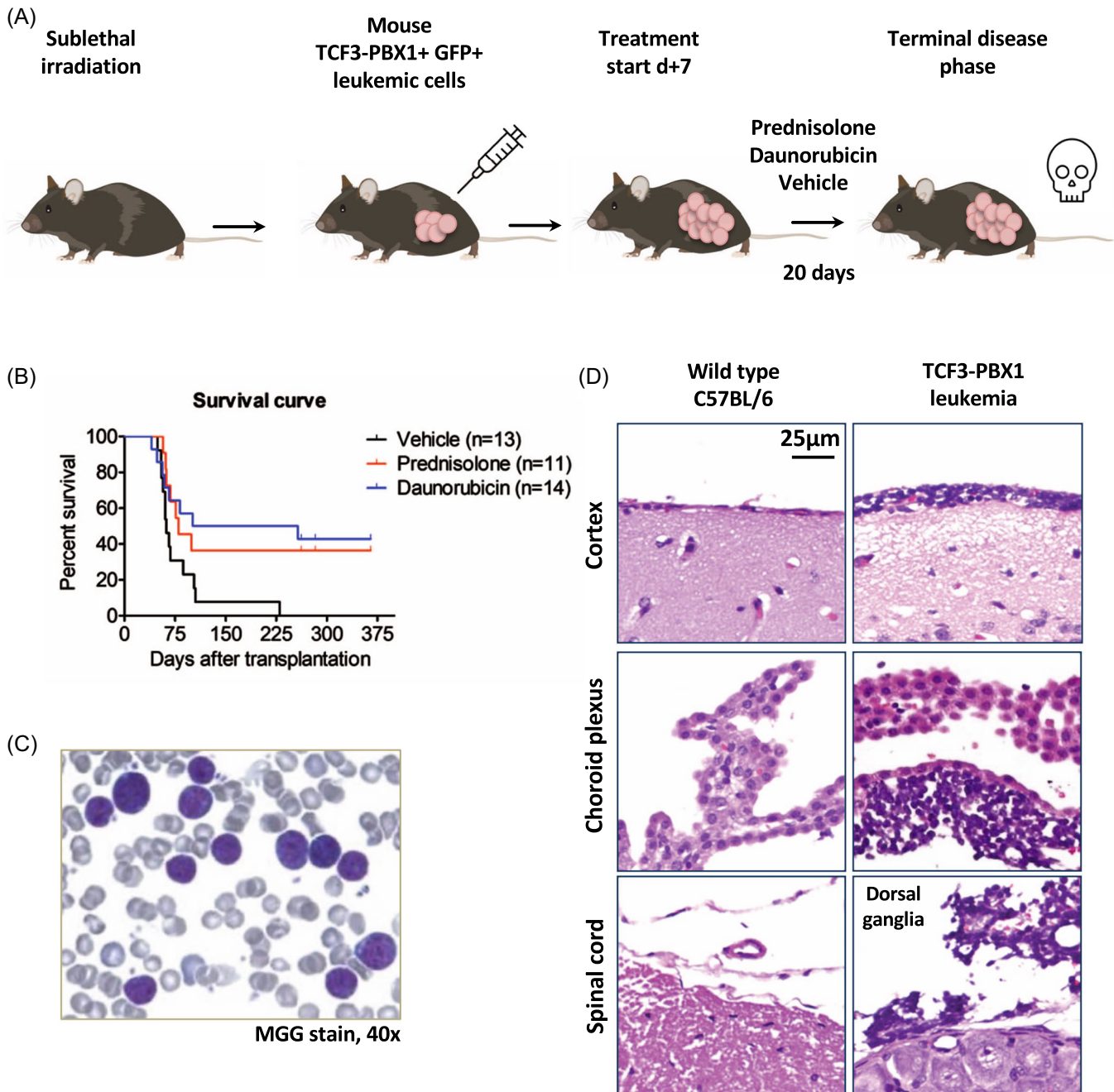

FIGURE 1 **Establishment of an in vivo mouse model to study relapsed disease after chemotherapy exposure depending on leukemia niche. (A)** Schematic illustration of experimental setup. Mice were sublethally irradiated and transplanted with 1000 GFP$^+$/TCF3-PBX1$^+$ leukemic cells. After engraftment, on Day 7, the mice were divided into three treatment groups: prednisolone, daunorubicin, and vehicle. Mice were treated i.p. for 20 days. After treatment, mice were monitored regularly and sacrificed when showing symptoms of leukemic disease. Isolated tissues were analyzed. **(B)** The Kaplan–Meier curve shows that 40% of the prednisolone-($n = 11$) or daunorubicin-($n = 14$) treated mice survive at least 270 days. Vehicle-treated mice ($n = 13$) died after a median survival of 62 days (log-rank test, $p < 0.05$). The experiment was performed three times with cohorts of five mice in each treatment group. Two vehicle-treated, four prednisolone-treated, and one daunorubicin-treated mice died of toxicity of the treatment or without leukemia cells and were excluded from final analysis. **(C)** Blood smear showing morphology of lymphoblasts from mouse TCF3-PBX1$^+$ leukemias (May–Grünwald Giemsa staining). **(D)** Hematoxylin and eosin staining of histological sections shows infiltration of TCF3-PBX1$^+$ leukemia cells in central nervous system tissues (cortex, choroid plexus, and spinal cord) compared to a wild-type control. Gy, gray; i.p., intraperitoneal; MGG, May–Grünwald Giemsa.
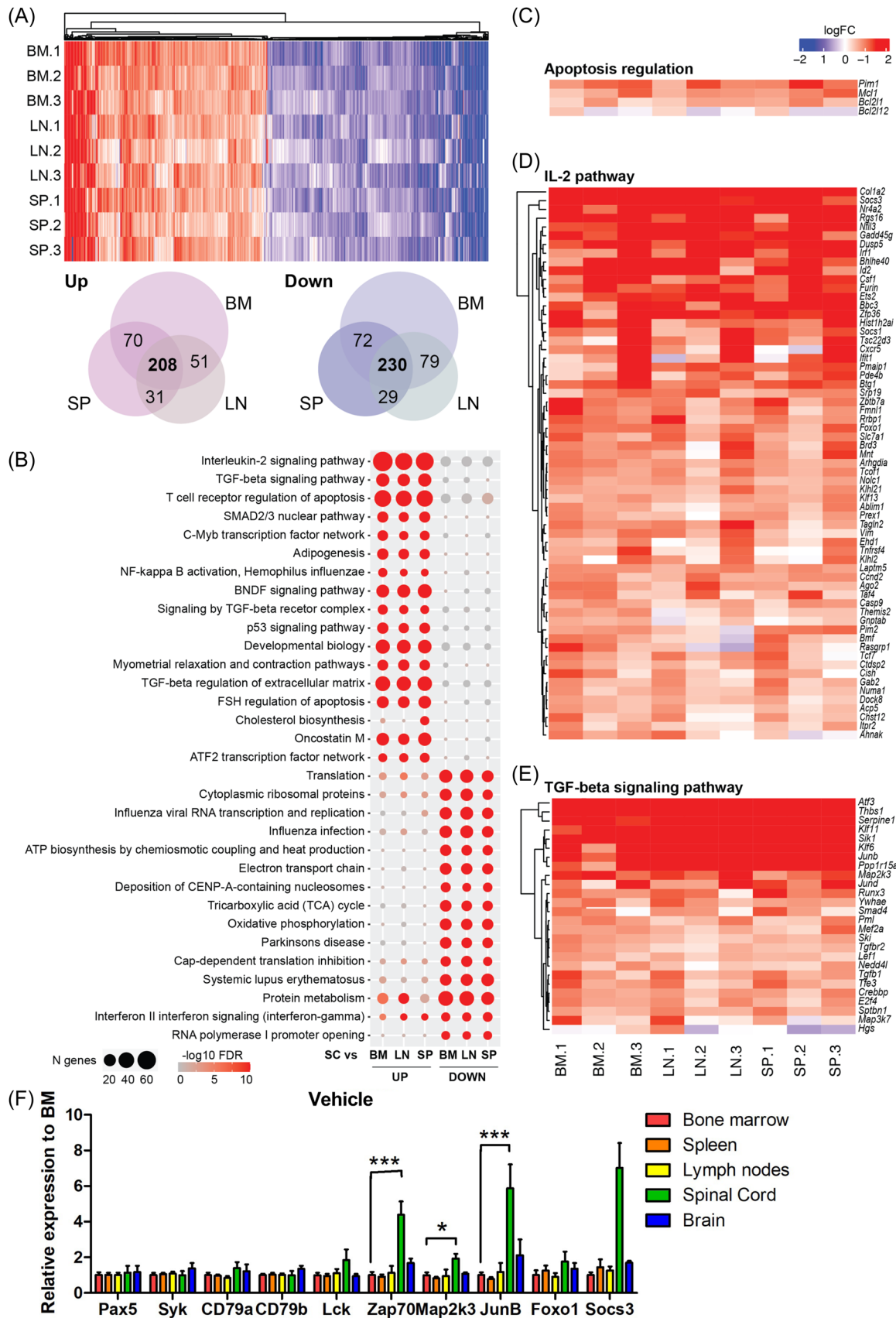
FIGURE 2 (See caption on next page).

FIGURE 2 Transcriptomic changes across tissue microenvironments in GFP$^+$ TCF3-PBX1$^+$ cells by bulk RNA sequencing. **(A)** Differentially expressed genes in GFP$^+$ TCF3-PBX1$^+$ leukemia cells infiltrating SC compared to BM, SP, and LNs with a $p < 0.05$ and log fold change (FC) > 0.6. Heatmap illustrating the gene expression level as log FC (e.g., tones of red indicate upregulation in SC, tones of blue downregulation in SC, no row scaling was used). Venn diagram displays common up and downregulated genes of SC-infiltrating leukemic cells. GFP$^+$ TCF3-PBX1$^+$ leukemic cells were isolated and FACS-sorted from specific organs from three different moribund mice from each treatment group. **(B)** Enrichment of biological top 10 processes in SC versus other tissues shown as dot plot. Size of the dot corresponds to the number of genes from the gene set and -log10 FDR value is shown in color, see also Supporting Information S1: Table S1. **(C–E)** Heatmaps illustrating the gene expression level as log FC (see Figure 2A) from apoptosis regulating genes and Enrichr Bioplanet upregulated pathways: IL2 and TGF-beta signaling. **(F)** Bar graph shows relative expression of genes in GFP + TCF3-PBX1$^+$ leukemic cells isolated from specific tissues and compared to BM in vehicle-treated mice quantified by RTqPCR. $\Delta\Delta C_T$ method and a two-sided Mann–Whitney test were used for statistical analysis. N, is depicted in the graph for each tissue as biological replicate. Each measurement by RT-qPCR was performed in technical triplicate. Error bars show the standard deviation. *$p < 0.05$; ***$p < 0.001$. BM, bone marrow; LN, lymph nodes; SC, spinal cord; SP, spleen.

results were filtered based on their adjusted p-values (<0.05) and visualized with dotplots made with ggplot2 (v.3.3.6).

Phospho-flow cytometry (Phospho-flow) and flow cytometry

Immunophenotyping was performed by flow cytometry following standard conditions. Antibodies for B220 (CD45R) (clone RA3-6B2), CD117 (clone 2B8), CD19 (clone 6D5), CD43 (clone S11), and CD45 (clone 30-F11) were purchased from BD Biosciences. Phospho-flow analysis was performed as described previously.[10] Acquisition was performed using a LSR Fortessa Cell Analyzer (BD Biosciences) with 10,000 events being acquired for each sample. Analysis was performed using the FlowJo Software v. 10.8.1 (BD Biosciences).

Real-time quantitative polymerase chain reaction (RT-qPCR)

RNA was isolated using the AllPrep DNA/RNA Mini Kit (Qiagen). RNA was reverse transcribed to single-stranded complementary DNA with SuperScriptIII Reverse Transcriptase and oligo (dT) 50 µM (Thermo Fisher Scientific). Taqman probes were obtained from Thermo Fisher Scientific. Gene expression was analyzed using the LightCycler® 480 RT-qPCR (Roche). Relative quantification of gene expression to either vehicle treated samples or BM of the same treatment was calculated using the $\Delta\Delta C_t$ method.

Mass cytometry (CyTOF)

CyTOF was performed according to previous work[24] and manual user guide from Standard Biotools Inc. Cells were stained with a panel of 28 antibodies including surface and intracellular markers (Standard Biotools Inc. and Supporting Information S1: Figure 12). Acquisition was performed on a CyTOF Helios and Hyperion 3rd generation (Standard Biotools Inc). OMIQ (Dotmatics) and FlowJo Software v. 10.8.1 (BD Biosciences) were used for analysis. Either opt-SNE (leukemic mice) or UMAP (wild-type mice) were applied for dimension reduction and FlowSOM was run to cluster similar populations (settings described in supplementary methods). CyTOF data were uploaded to FlowRepository (ID: FR-FCM-Z6K9).

Colony forming assays (CFAs)

Murine M159 (TCF3-PBX1$^+$/preBCR$^+$) and M1496 (TCF3-PBX1$^+$/preBCR$^-$) cell lines were cultured in M3234 Methocult (Stemcell Technologies Inc.), IMDM (Thermo Fisher Scientific Inc.), and murine Interleukin-7 (Peprotech US) in a final concentration of 10 µg/mL as previously described.[10]

Statistics

Survival curves were analyzed by a log-rank test. Statistical differences between 2 groups were analyzed with a two-sided nonparametric Mann–Whitney test or two-tailed Student t-test assuming a normal distribution or one-way analysis of variance. Statistical analysis of flow cytometry, RT-qPCR, drug sensitivity assays, and mass cytometry were performed using GraphPad Prism software, version 5.03 and 9.1.2 (Dotmatics). Dedicated bioinformatic packages and statistical approaches were used for single-cell data (see Supporting Information Methods).

RESULTS

Establishment of an experimental model to study relapsed leukemia cells under chemotherapy pressure depending on leukemia niche

To study mechanisms of relapsed disease after chemotherapy treatment, we performed secondary transplantation studies using preBCR$^+$/ TCF3-PBX1$^+$ leukemia cells derived from conditional TCF3-PBX1$^+$ knock-in mice (Figure 1A). Mice transplanted with TCF3-PBX1$^+$ GFP$^+$ leukemia cells and treated with vehicle succumbed to disease with a median survival of 62 days. We optimized chemotherapy drug concentration and transplantation conditions to allow about 40% of mice treated with prednisolone or daunorubicin to survive, thus mimicking the clinical situation of relapsed ALL (Figure 1B). Hence, leukemic mice developed clinical signs of ALL including CNS infiltration similar to human ALL (Figure 1C,D and Supporting Information S1: Figures 1 and 2). Chemotherapy-surviving TCF3-PBX1$^+$ leukemic cells showed a trend, although not statistically significant, for lower sensitivity (higher IC$_{50}$) to prednisolone and daunorubicin in ex vivo CFA (IC$_{50}$ prednisolone of TCF3-PBX1$^+$ leukemia from vehicle- vs. prednisolone-treated mice 3.7 vs. 4.5 nM, $p = 0.21$; IC$_{50}$ daunorubicin of TCF3-PBX1$^+$ leukemia from vehicle- vs. daunorubicin-treated mice 2.5 vs. 7.5 nM, $p = 0.12$) (Supporting Information S1: Figure 1D).

Inter-individual variation in the immunophenotype and genetically of TCF3/PBX1$^+$ leukemia cells upon chemotherapy treatment and microenvironment

No consistent differences were found in GFP$^+$ leukemic cells quantified by flow cytometry (Supporting Information S1: Figures 3 and 4) and in the known proB/early pre-B II immunophenotype (Supporting Information S1: Figure 5) in different tissues after vehicle or chemotherapy treatment. Nevertheless, major changes were observed in the immunophenotype of leukemias arising from single mice treated with daunorubicin or prednisolone in BM and LN as seen by a GFP$^+$
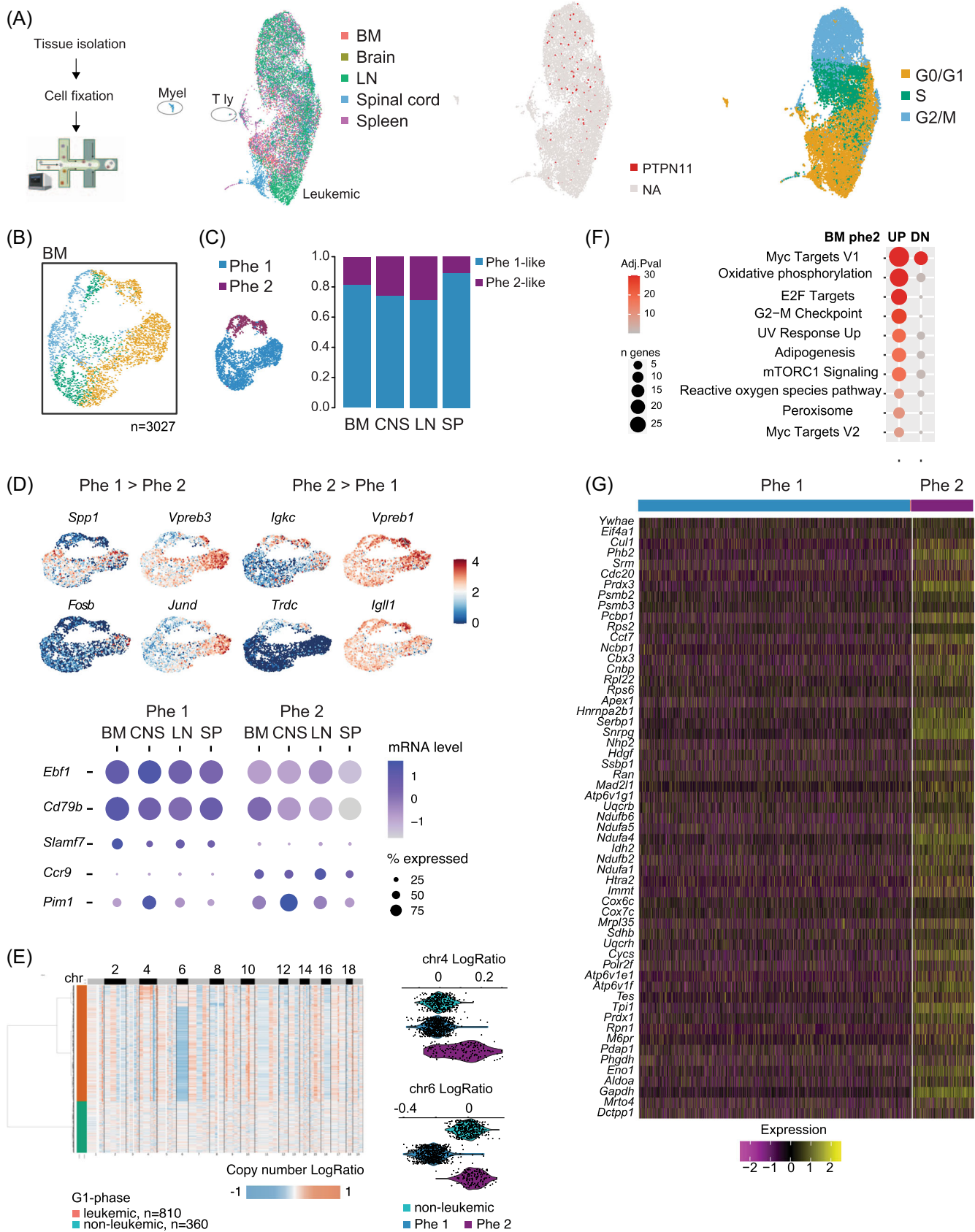
FIGURE 3 (See caption on next page).

FIGURE 3 Single-cell transcriptomic analysis distinguishes transcriptional and genetic heterogeneity within each tissue. **(A)** Left panel, Overview of the experimental setup for scRNAseq. Tissues from representative euthanized TCF3-PBX1$^+$ mice are isolated and cells fixed in formaldehyde before acquisition. *Middle and right panel*, Vehicle-treated tissues are shown on the UMAP plot. The predominant leukemic cells cluster together, while healthy blood cells, for example, myeloid cells and T-cells cluster separately. Colors correspond to different tissues (left) and PTPN11 mutation status (middle) and cell cycle phase (right). **(B)** Cell cycle phase in BM vehicle sample shown on UMAP (refer to Supporting Information S1: Figure 8 for CNS, LN, and SP). **(C)** Two distinct phenotypes across tissues in vehicle-treated samples. Two phenotypes are indicated on BM UMAP (left) and their proportions compared across tissues (right). **(D)** Upper panels, Phenotype 1 and 2 specific genes visualized on UMAPs (red color indicates higher expression, note cells in order of expression). Lower panels, Dotplot heatmap shows expression levels of phenotype specific genes (average expression level is indicated by tones of blue and dot sized represents percentage of cells expressing each gene). **(E)** Copy number estimates: Heatmap shows Log ratio to non-leukemic cells separated by chromosome for BM G1-phase cell (left). Blue denotes lower and red higher log ratio relative to reference nonleukemic cells (indicated in green). Violin plot shows LogRatio for chr 4 and chr 6 (right) comparing non-leukemic, Phe1, and Phe2 cells. **(F)** Dotplot visualization from Enrichment of biological top 10 upregulated processes (MSigDB Hallmark adj. *p* < 0.1) in vehicle-treated BM samples opposing the two phenotypes, see also Figure 2B and Supporting Information S1: Table S2. **(G)** Heatmap visualization of Myc targets and metabolic pathway genes (oxidative Phosphorylation and mTORC1 Signaling) from vehicle BM. Colors correspond to two different phenotypes (tones of violet indicate low-level expression, tones of yellow high level). BM, bone marrow; CNS, central nervous system (spinal cord and brain); LN, lymph nodes; Myel, myeloid cells; Phe 1, phenotype 1; Phe 2, phenotype 2; SP, spleen; T ly, T-lymphocytes. Number of cells analyzed is indicated below figure panels.

double-positive CD19$^+$/B220$^+$ cell population (Supporting Information S1: Figure 6A,B). Next, we tracked a PTPN11 G503A mutation, that we have previously identified in the m159 mouse leukemia cells in our experiments.[10] No significant changes in PTPN11 G503A VAF in vitro across the tissues (brain, SC, BM, spleen, LN) and within the different treatments were found (Supporting Information S1: Figure 6C).

Global transcriptome in TCF3-PBX1$^+$ leukemias depends on microenvironment

To gain insight into how the microenvironment influences the gene expression profile of CNS-infiltrating TCF3-PBX1$^+$ leukemias, we performed bulk RNAseq of GFP$^+$ sorted blasts from BM, SP, LN, and SC from three mice treated with vehicle. We compared leukemic cells residing in SC with BM, LN, and SP. We found 208 common upregulated genes and 230 common downregulated genes (log2 fold-induction >0.6, *p* < 0.05) (Figure 2A and Supporting Information S1: Table S1). Pathway analysis implicated significantly upregulated expression of the interleukin-2, TGF-β, and anti-apoptotic signaling pathway genes in leukemic cells residing in the SC (Figure 2B). SC leukemias showed elevated expression of *Socs3*, *Cish* (negative regulators of Stat-signaling), *Btg1* (suppression of proliferation); *Map2k3*, *Junb* (growth regulation); and *Mcl1* (anti-antiapoptotic) (Figure 2C–E). In comparison, several genes related to metabolic pathways (regulation of protein synthesis and oxidative phosphorylation) were downregulated (Figure 2B and Supporting Information S1: Figure 7A). We could also confirm that *Cd79a* was modestly upregulated (log2 fold change [FC] 0.59–0.62 in SC vs. BM and SP) in our mouse model similar to CNS-infiltrating human TCF3-PBX1$^+$ ALL[12] (Supporting Information S1: Figure 7B).

From the identified genes in bulk RNAseq analysis, as well as candidate genes involved in CNS infiltration in human ALLs, several genes were subjected to validation by RT-qPCR in GFP$^+$-sorted TCF3-PBX1$^+$ leukemia cells from a larger cohort of mice (*n* = 8). We confirmed higher expression levels for *Zap70* (*p* < 0.001), *Map2k3* (*p* < 0.05), and *Junb* (*p* < 0.001) and a trend for *Socs3* (*p* 0.057) in leukemia cells isolated from SC samples (Figure 2F and Supporting Information S1: Table S1).

Single-cell transcriptomes reveal two leukemic cell phenotypes present in each microenvironment

Changes in global transcriptional programs have been associated with chemotherapy resistance in leukemias.[25] To characterize whether

diversification of TCF3-PBX1$^+$ leukemic cells occurred in different tissues and under chemotherapy pressure, we next performed single-cell transcriptome measurements (scRNAseq) from cells isolated from BM, SP, LN, and CNS (brain and SC) from a representative mouse per treatment group. The leukemic cell-containing clusters were identified based on surface antigen expression and known *PTPN11* mutation status of leukemia cells (Figure 3A and Supporting Information S1: Figure 8A).[10] As an initial characterization, we quantified cell cycle activity using S- and G2/M-phase specific marker gene expression (Figure 3A (right) and Supporting Information S1: Figure 8B). Comparison of cell cycle state proportions revealed that leukemic blasts were actively cycling in each tissue, with only modest differences in the calculated cell proportions.

Next, leukemic cells were visualized separately from each tissue to compare cell state diversity. This analysis revealed additional heterogeneity within each tissue as shown in BM (Figure 3B) where two disjoint cycling cell populations were present (referred to as phenotype 1 and 2 hereafter) (Figure 3C). Both cell phenotypes were also found in the other tissues based on label transfer analysis where the phenotypes identified from BM were used as reference for anchoring and annotating matching cell populations in other tissues (Supporting Information S1: Figure S8D). The more predominant phenotype 1 represented, respectively, 82%, 74%, 71%, and 89% of cells within BM, CNS, LN, and SP in vehicle-treated samples (Figure 3C). Comparison of their gene expression profiles in BM identified 577 (Phe2: 397 up; 180 down) genes that significantly differed in their expression (Supporting Information S1: Table S2). Among these genes, we noticed that the predominating phenotype 1 cells displayed elevated expression of the *Cd79b* subunit of the BCR, surrogate light chain *Vpreb3*, immunomodulatory *Slamf7*, and the TFs *Ebf1* and AP-1 subunits *Fos* and *Jund*. Phenotype 2 cells had high expression of the light chain locus *Igkc*, surrogate light chains *Igll1* and *Vpreb1*, and interestingly transcribed also the TCR delta gene locus *Tcrd*. These cells also expressed *Ccr9* (C-C Motif Chemokine Receptor 9), the *Pim1* oncogene, and *Pax5* at higher levels (Figure 3D, Supporting Information S1: Figure 8C, and Supporting Information S1: Table S2).

To assess potential genetic clonality, we estimated copy numbers based on the scRNAseq data revealing that phenotype 1 may carry a loss of chr6 and phenotype 2 a gain of chr4 (Figure 3E and Supporting Information S1: Figure 8D). In confirmation, a large fraction of upregulated genes in phenotype 2 directly matched to chr4 and chr6 (such as *Igkc*, refer to Supporting Information S1: Table S2), corresponding to 21% and 48% of genes on these chromosomes detected with the scDD analysis; on average, only 2%–3% of genes in each chromosome showed differential expression. However, the differential expression of
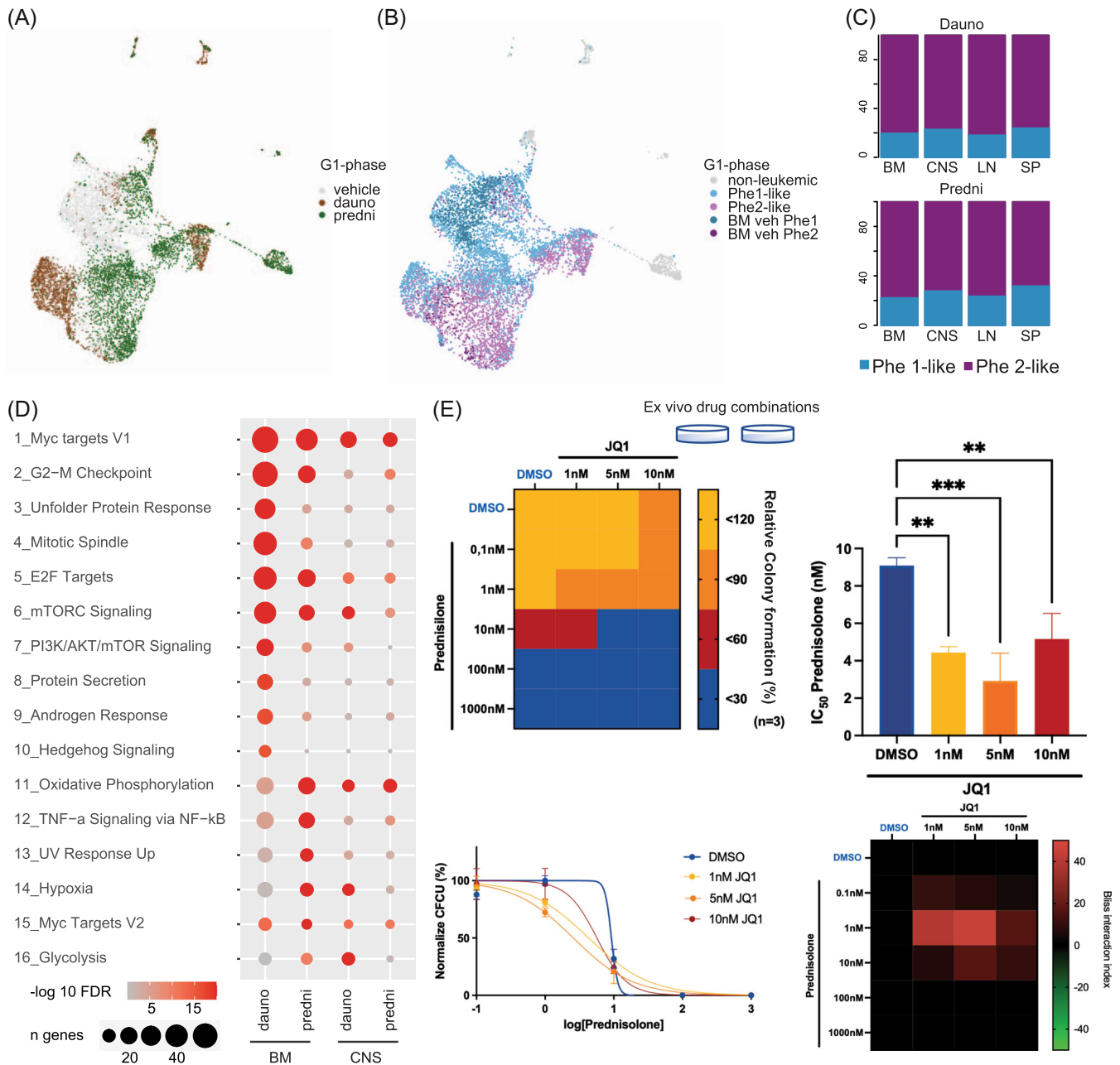
FIGURE 4 Myc active phenotype becomes predominant after chemotherapy pressure. (A) UMAP shows clustering across samples for cells in G1 cell cycle phase. Color denotes treatment group. (B) Phenotype labels indicated by color on the UMAP (left). BM vehicle cells were used as reference cells in label transfer. (C) Phenotype label proportion plot for all cells in treated samples (right). (D) Dotplot visualization from pathway enrichment analysis (dot size: number of genes; color: term significance). Enriched terms corresponding to upregulated genes (MSigDB Hallmark) in each treatment (daunorubicin or prednisolone) are shown comparing BM and CNS tissue, see also Supporting Information S1: Table S2. (E) Left upper panel, heatmap represents reduction of clonogenicity by the combination treatment of low-dose JQ1 and prednisolone compared to vehicle-treated TCF3-PBX1^{+} leukemia cells. Right upper and left lower panels, titration curves represent CFA of TCF3-PBX1^{+} leukemia cells treated with a combination of JQ1 and prednisolone. JQ1 reduced the IC50 of prednisolone significantly ($p = 0.0003$). Data show the IC_{50} calculated using nonlinear regression analysis and curves were compared with the sum-of-squares F test. Dose-response curves of each JQ1 concentration were compared to the dose-response curve of the vehicle-treated cells as controls ($n = 3$). Error bars represent the standard deviation. Lower right panel, bliss interaction index between JQ1 and prednisolone is shown. ns not significant; **$p < 0.01$; ***$p < 0.001$. dauno, daunorubicin; Phe 1, phenotype 1; Phe 2, phenotype 2; predni, prednisolone.

a subset of markers, including the BCR-signaling-related *Vpreb1* and *Igll1*, did not directly relate to location on chr4 or chr6.

At the pathway level, phenotype 2 showed higher *Myc* and *E2F* target gene expression, together with high expression of *mTorc* and oxidative phosphorylation pathway-related genes (Figure 3F,G). The

enrichment of Myc motif and known Myc target genes remained significant when examining the expression changes that did not map to chr4 and chr6. *Mycbp*, an upregulated gene encoded on chr4, could represent a putative effector gene related to more pronounced Myc activation. Interestingly, despite the higher Myc activity, metabolic
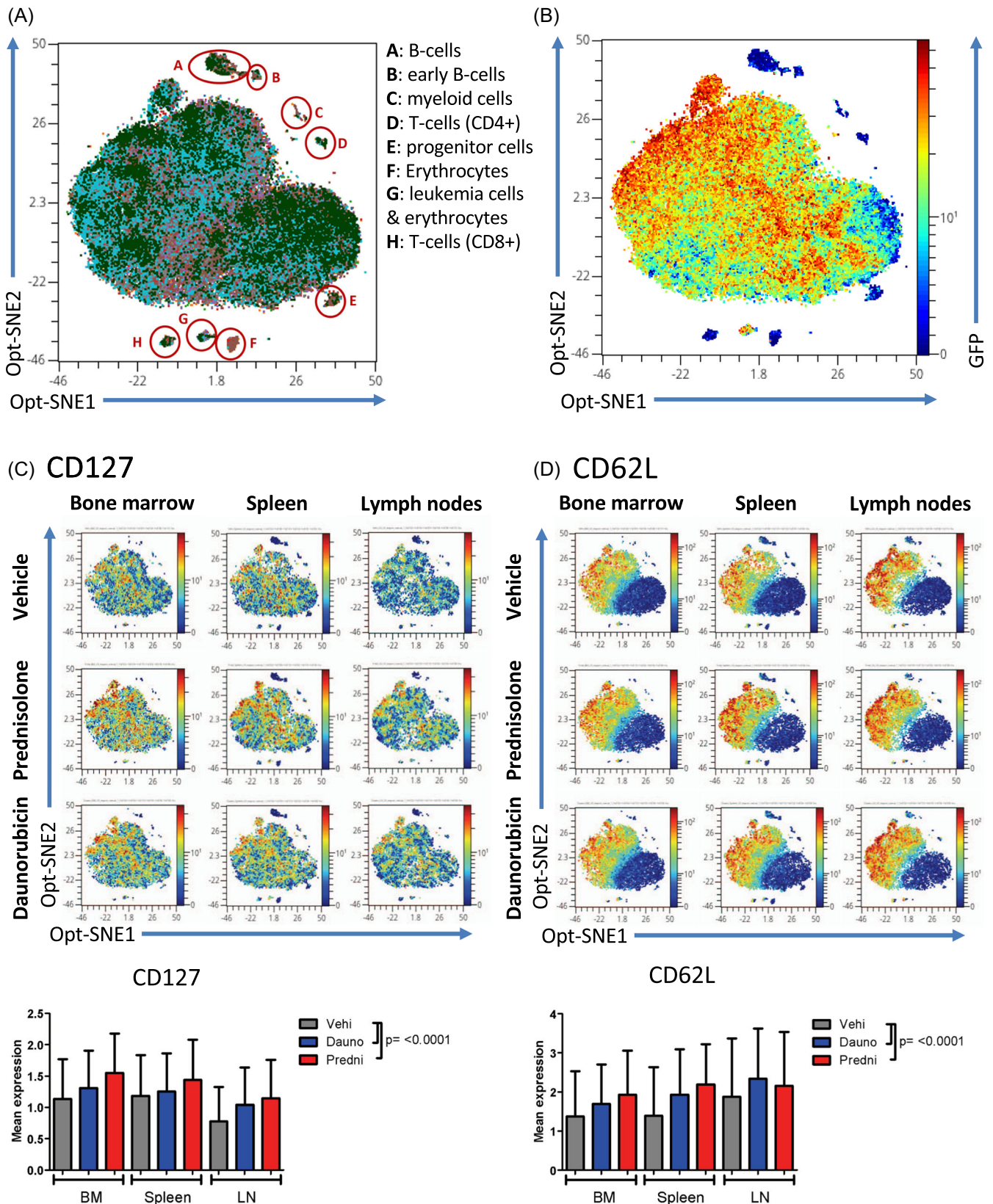
(A)

A: B-cells
B: early B-cells
C: myeloid cells
D: T-cells (CD4+)
E: progenitor cells
F: Erythrocytes
G: leukemia cells & erythrocytes
H: T-cells (CD8+)

(B)

(C) CD127

(D) CD62L

FIGURE 5 (See caption on next page).

FIGURE 5 Clonal dynamics of TCF3-PBX1^{+} leukemias at the protein level by single-cell mass cytometry (CyTOF) in different tissues under chemotherapy pressure. (A) Opt-SNE visualization of unstimulated samples reveals large cluster of GFP^{+} leukemic cells in the middle of the panel along with smaller clusters of healthy blood cells (GFP-negative), for example, B-cells, T-cells, and myeloid cells in the periphery. Tissues BM, SP, and LN from a representative mouse from each treatment group are shown ($n = 9$ samples). Each color represents a different sample. Clustering does not differ in between the samples. (B) Opt-SNE visualization of heterogeneous GFP expression of unstimulated TCF3-PBX1^{+} leukemic cells. (C, D) Some examples from regulated proteins depending on treatment and/or microenvironment are shown. (C) Upper panel, opt-SNE visualization of the upregulated expression of the IL7-receptor (CD127) and (D) SELL (CD62L) after treatment with prednisolone and daunorubicin. TCF3-PBX1^{+} leukemia cells from lymph nodes show a decreased expression of CD127 but an increased expression of CD62L. (C, D) Lower panels show the quantification of protein expression depending on treatments (vehicle, prednisolone, daunorubicin) and microenvironments (BM, SP, LN). Bars represent the mean expression and error bars the standard deviation. Statistics are calculated using a two-sided Mann–Whitney test. BM, bone marrow; Dauno, Daunorubicin; Predni, Prednisolone; LN, lymph nodes; SP, spleen; Vehi, Vehicle.

capacity, and proliferative pathway expression, phenotype 2 corresponded to the smaller cell population in vehicle-treated cells.

Regulation of MYC targets characterizes TCF3-PBX1^{+} leukemias under chemotherapy pressure representing a vulnerability to BRD3/4 inhibition

The tissue-specific gene expression changes and presence of cell phenotype diversity at transcriptional and clonal level prompted the analysis of leukemias exposed to chemotherapy drugs. Consistently across tissues, we noticed that cells resembling phenotype 2 with high *Myc* target expression became the predominant cell phenotype present after chemotherapy (Figure 4A–C and Supporting Information S1: Figure 9A,B). At the pathway level, this similarity corresponded to enrichment of *Myc* targets, oxidative phosphorylation, and apoptosis regulation-related genes (Figure 4D, Supporting Information S1: Figure 9C, Supporting Information S1: Table S2, see also the cluster-level comparison in Supporting Information S1: Table S2). Based on CNV analysis, correspondingly, the prevalence of chr6 deletion that distinguished phenotype 1 at CNV level in vehicle animals decreased (Supporting Information S1: Figure 9D). However, only a subpopulation of leukemic cells that matched to phenotype 2 carried the chr4 amplification, indicating that convergence toward this transcriptional phenotype could occur in genetically diverse leukemic populations (Supporting Information S1: Figure 9D). Indicating possible treatment resistance, chemotherapy-surviving leukemic cells upregulated the antiapoptotic genes (*Mcl1* upon prednisolone and *Bcl2l2* upon daunorubicin), AP-1 complex gene expression (*Junb*, *Jund*, *Fos*, *Fosb*), and *Il7r* that characterized CNS-infiltrating leukemia cells (Supporting Information S1: Figure 9A–C). In comparison, the pre-BCR gene expression (*Igll1*, *Vpreb1*, *Vpreb3*) was repressed in BM and CNS (Supporting Information S1: Figure 9C). Hence, we conclude that genetic selection of resistance mutations/CNV may have occurred in the timeframe of drug exposure and is likely to play a minor role in the survival of relapsed clones. Nevertheless, coexisting transcriptional adaptations found may represent a transient and reversible phenotype shift leading to relapsed disease.

As Myc target expression was highest in the chemotherapy-surviving cells of phenotype 2 and further upregulated upon treatment, we hypothesized that pharmacologically downregulated MYC expression could reduce required doses of chemotherapy to minimize toxicity. Inhibition of BRD3/4 by small molecules has been shown to repress MYC and subsequently, its target genes in ALL depending on MYC.[26] To test this in an ex vivo model, we treated murine TCF3-PBX1^{+}/preBCR[+] m159 (same leukemia as profiled in vivo) with the BRD3/4 inhibitor JQ1 alone, confirming reduced expression levels of *Myc* (Supporting Information S1: Figure 10A) and reduced clonogenicity of TCF3-PBX1^{+} leukemia cells (Supporting Information S1: Figure 10B,C). Combinatorial treatment with JQ1 and prednisolone significantly reduced the IC50 value of prednisolone ($p < 0.05$, AUC for DMSO 2453, 1 nM JQ1 2208,

5 nM JQ1 1453, 10 nM JQ1 1425), revealing an additive effect as seen by bliss interaction index[27] (Figure 4E). Similar effects (however, not statistically significant) were observed with the combination treatment of JQ1 with daunorubicin (Supporting Information S1: Figure 10D). Then, we performed CFAs with TCF3-PBX1^{+} leukemia cells isolated from vehicle- and chemotherapy-treated mice. We found that sensitivity to chemotherapy in combination with JQ1 was similar regardless of previous treatment suggesting a therapeutical benefit even in relapsed disease (Supporting Information S1: Figure 10E).

Mass cytometry (CyTOF) reveals phenotypic diversity and changes at the protein level with increased STAT3/5 phosphorylation

To elucidate the hierarchical structure of hematopoietic cells, interaction of leukemic cells with the microenvironment, and changes in protein expression and signaling response to chemotherapy treatment in vivo, we performed mass spectrometry (CyTOF) using a panel of 28 conjugated antibodies and palladium isotopes as barcodes (Supporting Information S1: Figures 11 and 12). Due to high cell loss in CNS tissues while processing the samples, we focused our analysis on BM, spleen, and LN and exclude CNS samples from final analysis. Using phenotypic markers, small clusters of healthy blood cells such as CD4+ and CD8 + T-cells, myeloid progenitor cells, and erythrocytes could be distinguished from GFP^{+} leukemic cells (Figure 5A,B). Concordant with scRNAseq, the leukemic cells showed heterogeneity that was already present in vehicle-treated cells visible as heterogenous expression of GFP, CD43, CD79a, CD79b, CD117, and Pax5 (Supporting Information S1: Figures 13 and 14). Cells treated with prednisolone and daunorubicin showed a higher expression of CD127 (encoded by Interleukin 7 receptor (*Il7r*); $p < 0.0001$, FC comparison Vehi vs. Pred 1.37, Vehi vs. Dauno 1.18) and CD62L (*Sell*) ($p < 0.0001$, FC comparison Vehi vs. Pred 1.38, Vehi vs. Dauno 1.22) in basal state compared to vehicle-treated cells (Figure 5C,D), concordant with similar changes observed in scRNAseq (Supporting Information S1: Figure S9).

We next analyzed changes in surface, cytoplasmic, as well as in phosphorylated protein expression after preBCR-signaling stimulation in GFP[+] leukemic blasts (Figure 6A,B). FlowSOM clustering across BM, SP, and LN cells revealed three main clusters of cells: Cluster 1 representing the unstimulated samples and Cluster 2 and 3 dividing the stimulated samples (Figure 6B and Supporting Information S1: Figure 15A). Upon stimulation, only Cluster 3, but not Cluster 2, reacted to stimulation by increasing phosphorylation with an expansion of Cluster 3 in cells from chemotherapy-treated mice (Figure 6B and Supporting Information S1: Figure 15B). Median expression of proteins differed in the three clusters (Supporting Information S1: Figure 15C).

Leukemic cells, independent of in vivo treatment with vehicle, prednisolone, and daunorubicin, reacted with a decrease of surface proteins CD117, CD62L, and CD127 ($p < 0.0001$, FC comparison US vs. preBCR in BM for CD117: Vehi 0.73; Dauno 0.51; Pred 0.58. For CD62L: Vehi 0.62,
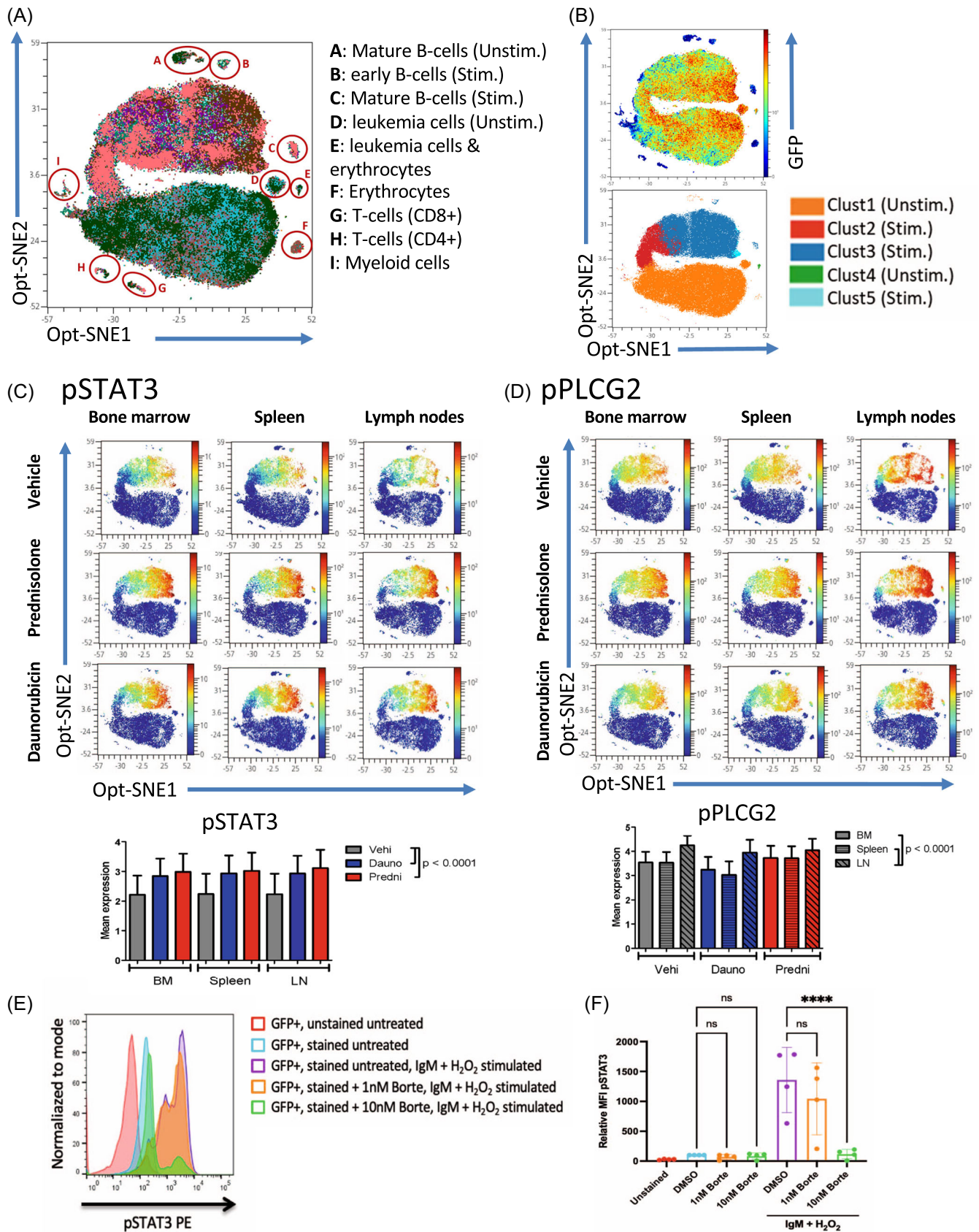
FIGURE 6   (See caption on next page).

FIGURE 6 Activation of signaling pathways of TCF3-PBX1$^+$ leukemias upon preBCR stimulation at the protein level in different tissues under chemotherapy pressure. **(A)** Opt-SNE visualization of unstimulated and preBCR-stimulated (IgM + H_2O_2) cells. TCF3-PBX1$^+$ leukemia cells from unstimulated and preBCR-stimulated samples cluster together in the middle with a concentration of stimulated cells in the top half and unstimulated cells in the lower half of the panel. Healthy cells (GFP negative) including early and mature B-cells, cluster in the periphery. Tissues BM, SP, and LN from a representative mouse from each treatment group with and without preBCR stimulation are shown (n = 18 samples). Each color represents a different sample. Clustering does not differ in between the samples. **(B)** Upper panel, opt-SNE diagram shows GFP expression. Heterogeneous GFP expression in TCF3-PBX1$^+$ leukemia cells does not differ between stimulation conditions. Lower panel, FlowSOM Clustering identifies three major clusters of leukemic cells after gating for GFP$^+$ cells only: Cluster 1 represents the unstimulated cells. Cluster 2 and 3 divide the stimulated samples, with Cluster 3 being predominant. **(C)** Upper panel, phosphorylation of STAT3 after preBCR stimulation is increased in Cluster 3 in all analyzed tissues (BM, SP, and LN) after treatment with prednisolone or daunorubicin compared to vehicle treatment. **(D)** Upper panel, phosphorylation of PLCG2 after preBCR stimulation is increased in Cluster 3 in LN compared to BM and SP. No differences of pPLCG2 after preBCR stimulation were observed after treatments. **(C, D)** Lower panels show the quantification of protein expression depending on treatments (vehicle, prednisolone, daunorubicin) and microenvironments (BM, SP, LN). Bars represent the mean expression and error bars the standard deviation. Statistics are calculated using a two-sided Mann–Whitney test. **(E)** STAT3-phosphorylation is assessed in vitro in unstimulated and preBCR stimulated TCF3-PBX1$^+$ cells (M159) after pretreatment with bortezomib at different concentrations by phosphoFlow. Median Fluorescence Intensity (MFI) of pSTAT3-PE is visualized as histograms. **(F)** Relative MFI to DMSO is shown (n = 4), statistical analysis is performed by one-way analysis of variance. Bars represent the mean and error bars represent the standard deviation. ns, not significant; ***$p < 0.0002$, ****$p < 0.0001$. BM, bone marrow; Borte, Bortezomib; Dauno, Daunorubicin; LN, lymph nodes; Predni, Prednisolone; SP, spleen; Vehi, Vehicle.

Dauno 0.47, Pred 0.52. For CD127: Vehi 0.86; Dauno 0.65; Pred 0.66) (Supporting Information S1: Figure 16). Interestingly, increased phosphorylation of STAT3 and STAT5 could be detected in prednisolone- and daunorubicin-treated mice compared to vehicle-treated mice (pSTAT3 $p < 0.0001$, FC comparison US vs. preBCR BM: Pred 1.34, Dauno 1.28. pSTAT5 $p < 0.05$, FC comparison US vs. preBCR Pred 1.17, Dauno 1.01) upon preBCR stimulation (Figure 6C and Supporting Information S1: Figure 17). PreBCR stimulation also resulted in an increase of SCA1, CD79b, PAX5, pLCK, pZAP70/pSYK, and pERK across all treatments (Supporting Information S1: Figures 17 and 18). The microenvironment influences the phosphorylation state of leukemia cells as seen by the increased phosphorylation of PLCG2 in LN compared to BM and SP ($p < 0.0001$, FC comparison vehicle-treated LN vs. BM & Spleen) (Figure 6D).

Identification of signaling pathways upstream of pSTAT3/pSTAT5 upon preBCR stimulation

To identify which pathways are activating STAT3 and STAT5 after preBCR stimulation, we performed phospho-flow and CFA experiments in the presence of potent signaling pathways inhibitors in vitro (Figure 6E,F and Supporting Information S1: Figure 19). First, we hypothesized that the JAK kinases are upstream of STAT3/5, knowing their important role in our and other B-ALL mouse models.[10,28] No changes in STAT3 or STAT5 phosphorylation were observed after pretreatment with the JAK1/2 inhibitor ruxolitinib and preBCR stimulation (Supporting Information S1: Figure 19A). The proteasome pathway has been involved in STAT3 and STAT5 phosphorylation after BCR activation in mantle cell lymphoma.[29] In earlier works, we have elucidated the importance of TGF, mTOR, and PI3K/AKT pathways in leukemic transformation.[30,31] Comparing the inhibition of these pathways showed that preincubation of TCF3-PBX1$^+$ leukemia cells with the proteasome inhibitor bortezomib significantly inhibited induction of pSTAT3 and pSTAT5 after preBCR stimulation, while inhibition with Capivasertib, Torin1, and TGF-β of harvested leukemic cells derived from BM was not able to suppress phosphorylation of STAT3 and STAT5 (Figure 6E,F and Supporting Information S1: Figure 19B,C).

Higher PAX5 levels and phosphorylation of ERK and ZAP70/SYK distinguishes the response of TCF3-PBX1$^+$ leukemia cells from wild-type B-lineage mouse cells

To better understand the mechanisms underlying changes in cell signaling after exposure to chemotherapy agents or microenvironment,

we wanted to explore whether the differences in antigen expression and induction of phosphorylation are related to the transformation of the TCF3-PBX1$^+$ leukemia cells or are related to the stage of differentiation. We analyzed pooled BM and SP samples from 2 wild-type mice using the same panel of CyTOF antibodies. In the wild-type samples, distinct populations clustered symmetrically with opposing stimulation conditions. FlowSOM Clustering revealed 11 different clusters of cellular populations, for example, mature B-cells in cluster 03, early B-cells (CD19+, IgM−) in cluster 11 (CD127+) and cluster 10 (CD127−), and progenitor B-cells in cluster 08 (CD117+, CD43+), as well as populations of other lineages (Figure 7A–C and Supporting Information S1: Figure 20).

As expected, (pre)BCR stimulation by H_2O_2 and IgM was effective and could be assessed by increased phosphorylation with the strongest stimulation response in mature B-cells (Figure 7D and Supporting Information S1: Figure 20C). Of note, PAX5 was substantially lower expressed in wild-type B-lineage cells (cluster 03 and 11) than in TCF3-PBX1$^+$ leukemic cells (early B-cells BM wt vs. vehi $p < 0.001$, FC comparison BM US 2.21; Figure 7D,E and Supporting Information S1: Figure 21A,B). Furthermore, there was less phosphorylation of ERK, ZAP70/SYK, STAT3, and STAT5 upon (pre)BCR stimulation in B-cells from wild-type mice when compared to TCF3-PBX1$^+$ leukemia cells, indicating an acquisition of aberrant signaling pathways in leukemia cells (FC comparison US vs. preBCR in BM pERK: vehi 2.4, early B-cells wt 3.7; pZAP70/pSYK: vehi 8.5, early B-cells wt 6.6; pSTAT3: vehi 17.1, early B-cells wt 12.6; pSTAT5: vehi 21.2, early B-cells wt 13.4; Figure 7D,E and Supporting Information S1: Figure 21). Overall, we found that TCF3-PBX1$^+$ leukemias have a lower expression of CD45 (FC Vehi vs. early wt 0.97) and CD19 (FC vehi vs. early B-cells wt 0.63) than wild-type cells regardless of their developmental state, and a higher expression of CD43, CD117, CD62L, and PAX5 (FC vehi vs. early B-cells wt CD43: 1.58; CD117 16.9; CD62L 1.23; PAX5 2.21; Figure 7E). Thus, we could show that while some changes in protein expression are related to the developmental state, leukemic transformation regulates several proteins and signaling pathways in our TCF3-PBX1$^+$ mouse model.

DISCUSSION

Previous studies have revealed that both resistance mutations and more drug-tolerant cell phenotypes, regulated by gene regulatory and signaling networks, can impact drug responsiveness.[32] This heterogeneity in cell states and mutation profiles prompts studying leukemia drug response at single-cell resolution.[33,34] Preclinical models are best-suited to systematically investigate the phenotypic diversity
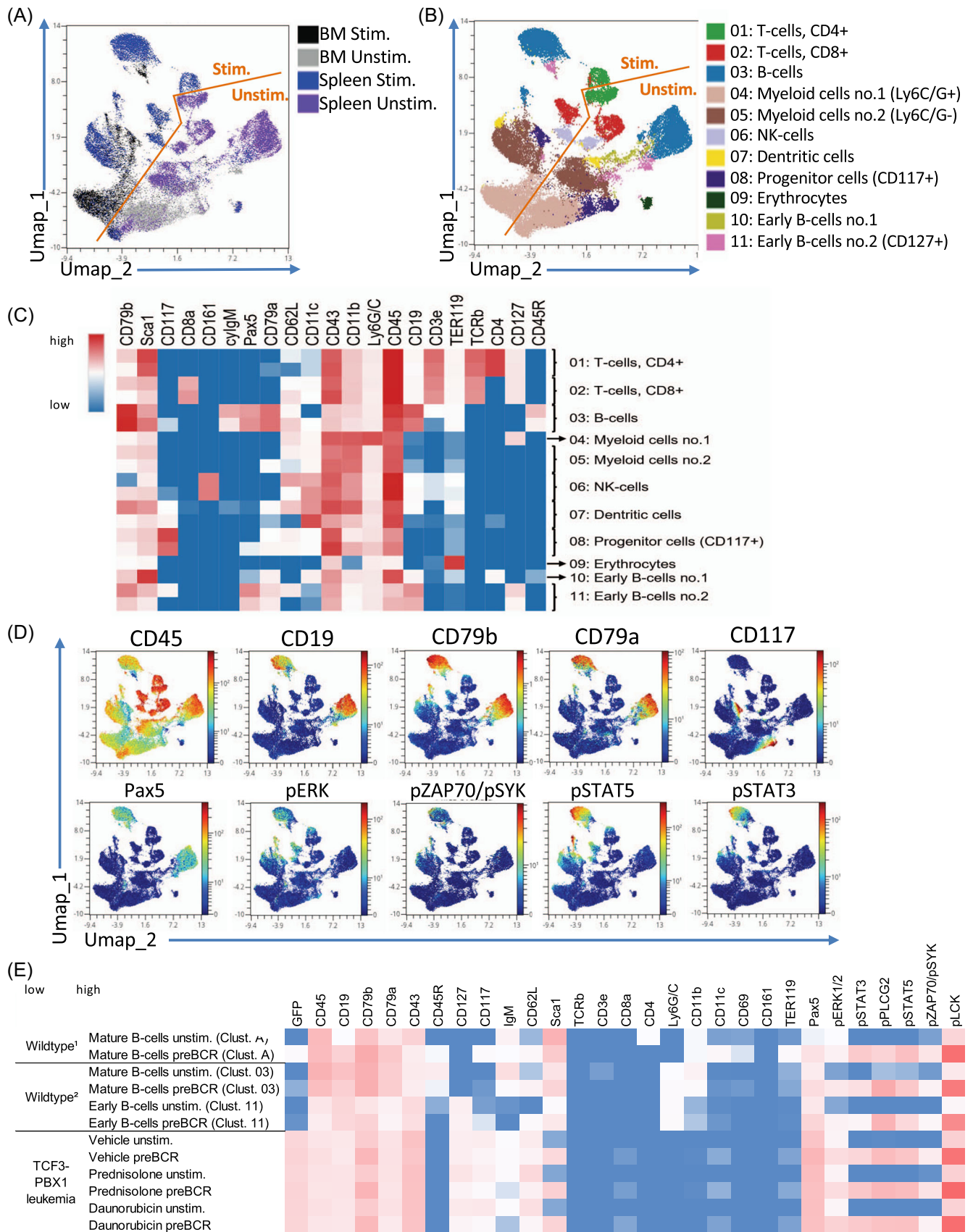
FIGURE 7 (See caption on next page).

FIGURE 7 Activation of signaling pathways in bone marrow cells from wild-type mice upon preBCR stimulation at the protein level. **(A)** UMAP visualization of unstimulated and preBCR-stimulated (IgM + H_2O_2) samples of bone marrow and SP from two pooled wild-type mice symmetrically opposed. **(B)** FlowSOM Clustering identifies 11 different clusters including B-, T-, NK-, myeloid, and progenitor cells. **(C)** Heatmap shows surface and intracytoplasmatic protein expression of clusters identified via FlowSOM Clustering. Related clusters of opposing stimulation conditions cluster next to each other. **(D)** UMAP visualization of surface, intracytoplasmatic, and phospho-protein expression in clusters define cellular populations depending on tissue (BM, SP) and preBCR stimulation. Of note, expression of pZAP70/pSYK and pERK after preBCR stimulation and PAX5 is weaker in healthy pro B- and mature B-cells compared to TCF3-PBX1^{+} leukemia cells (see Supporting Information S1: Figure 21). **(E)** Heatmap reveals differences in median protein expression in bone marrow between mature B cells[1] from leukemic mice (Cluster A), early and mature B cells[2] from wildtype mice (Cluster 03 and 11) and TCF3-PBX1^{+} leukemic cells as can be seen in mass spectrometry. BM, bone marrow; SP, spleen; Stim, preBCR-stimulated; Unstim, unstimulated.

induced by drugs in vivo.[35] Different methods to analyze leukemic cells at a single cell level allowed us to show the influence of the microenvironment and chemotherapy treatment. Leukemic cells showed considerable heterogeneity and plasticity at transcriptome, copy number, and signaling level in response to tissue microenvironment, drug exposure, and stimulation.

Recent work has uncovered factors, which may allow ALL cells to migrate to the CNS,[36] including metabolic plasticity to use lipids in low oxygen microenvironments.[37] The microenvironment plays an important role in leukemia progression[38] and chemotherapy resistance.[39,40] Mechanisms shown to protect cells from methotrexate and glucocorticoids in CNS involve cell–cell interaction (via Mertk-galectin, or Itga4-Vcam1) that induce quiescence[9,41] or anti-apoptotic gene levels.[42] Direct target genes of leukemic fusion proteins may play a role in this mechanism.[43,44] We established conditions to study TCF3-PBX1^{+} ALL leukemia after in vivo chemotherapy treatment in our mouse model depending on niche. In line with human studies, the expression of anti-apoptotic Mcl-1 was highest in CNS-infiltrating leukemic cells. Other genes associated with relapsed ALL in CNS[9,12,13,43,45,46] including ZAP70, IL7R, CD79a, and CD79b were also upregulated on the messenger RNA and/or protein level. Altogether, we show that our TCF3-PBX1^{+} leukemia mouse model reflects similarities with CNS-infiltrating human TCF3-PBX1^{+} leukemias. However, the CNS-infiltrating phenotype was not associated with Mertk (not detected) expression in the mouse leukemias.

At the signaling pathway level, the activated JAK/STAT signaling and constitutive activation of the RAF/RAS/MEK/ERK pathway have been described to be associated with ALL blasts infiltrating CNS.[36,47,48] Our transcriptome profiles implicated high expression of genes involved in the TGFβ signaling pathway in TCF3-PBX1^{+} leukemia cells infiltrating CNS compared to BM-, SP-, and LN-infiltrating leukemia cells. Interestingly, we have recently described the involvement of the TGFβ signaling pathway in ALL[31] and resistance to targeted therapies as the tyrosine kinase inhibitor dasatinib[49] suggesting a central role of this pathway in TCF3-PBX1^{+} leukemias. Several signaling proteins were enriched after exposure to prednisolone such as CD79b and IL7R (CD127) as well as phosphorylation of STAT3 and STAT5 underlying the importance of the JAK-STAT pathway in this leukemic model according to recent data.[50] Stimulation of the preBCR prompted an increased expression of CD79b, but a downregulation of the Il7R, suggesting plasticity and ability to switch between two major signaling pathways in order to maintain survival.[51] Additionally, treatment with chemotherapy increased the number of cells that were sensitive to preBCR stimulation, suggesting a survival advantage. Previous work revealed that preBCR-expressing leukemias are susceptible to inhibition of kinases downstream of the preBCR.[52] We showed that the proteasome pathway is involved in the preBCR-induced phosphorylation of STAT3 and STAT5 in TCF3-PBX1^{+} leukemia similar to previous observations in mantle cell lymphoma.[29] The inhibitory effect of bortezomib on STAT3/5 phosphorylation might depend on disruption of the autocrine secretion loop of IL6 and IL10, and a possible connection of NF-κB and STAT3 signaling, in the context of BCR stimulation in mantle cell lymphoma.[29] Interestingly, bortezomib in combination with

chemotherapy showed high activity in patients with relapsed ALL with different karyotypes treated in a clinical trial.[53] Exploration of additional upstream pathways such as JAK-, PI3K/AKT-, TGFβ-, and mTOR pathway did not result in reduction of pSTAT3/5 after pre-BCR stimulation in our mouse model.

Single-cell transcriptomics revealed that engrafted leukemias exhibited genetic and transcriptomic diversity. We found cells characterized by enrichment in the AP-1 transcriptional network predominantly in vehicle-treated samples. In each tissue, cells with enrichment in Myc and E2F transcriptional networks were also present. Copy number analysis associated part of this gene expression profile difference with differential chr4 and chr6 copy number levels. In drug-treated samples, leukemic cells were further diversified at copy number level. However, convergence to high Myc activity state was consistent in drug-exposed leukemias. Similar canalization of phenotype has been previously reported in xenograft experiments.[54] Inhibition of deregulated *Myc* expression through BRD3/4 inhibitor JQ1 and its anti-proliferative effects on different types of malignancies have been reported in several studies.[55,56] In our TCF3-PBX1^{+} leukemia model, JQ1 repressed Myc expression and increased sensitivity to prednisolone and daunorubicin treatment in CFA with primary TCF3-PBX1^{+} leukemic cells and in leukemias arising after *in vivo* chemotherapy treatment, thereby suggesting a role of BRD3/4 inhibitors in primary and relapsed ALL disease. Future experiments should be carried out to establish combination therapies in vivo addressing how this initial sensitivity could be optimally exploited with more stable BRD3/4 inhibitors suitable for clinical use.

This study has some limitations. We were not able to analyze clonal genetic selection at single nucleotide variant level, due to the technical limitations of scRNA-seq, except by tracking the formerly detected leukemia-driving mutation PTPN11 G503A[10] and CNV analysis. Inclusion of WGS or WES in future studies would enable tracking both transcriptional and genetic diversity. This work is also limited by the number of mice included in single-cell analysis by scRNAseq and mass spectrometry. However, the in-depth characterization of regulated pathways by a broad spectrum of methods including transcriptomics, protein phosphorylation, and CFA allowed us to obtain a deeper understanding of leukemic cell diversity that future studies can leverage. Follow-up analysis of the identified pathways is needed to further elucidate resistance mechanisms contributing to relapsed disease. Finally, the combination therapies should be examined using larger in vivo cohorts for optimizing drug timing to prevent drug resistance and disease recurrence.

In summary, we have developed a mouse leukemia model for characterizing relapsed clones after in vivo chemotherapy exposure depending on cell-extrinsic microenvironment effects and cell-intrinsic factors attributable to differential TF and signaling activity as well as sub-clonal diversity. Transcriptomics and phospho-proteomics at the single-cell level elucidated key pathways underlying cell phenotype plasticity and identified TF- and signaling pathway-dependent mechanisms of chemotherapy resistance, which might be suitable for pharmacological therapies in human ALL.

AUTHOR CONTRIBUTIONS

Jesús Duque-Afonso and Merja Heinäniemi involved in study design. Mira Kusterer, Mari Lahnalampi, Minna Voutilainen, Alexandra Brand, Sandra Pennisi, Johana Norona, Heike Herzog, Mikko Sipola, Emma Kaartinen, Roman Sankowski, Marco Prinz, Saskia Killmer, Marilyn S. Lago, Stepan R. Cysar, Konrad Aumann involved in data collection. Mira Kusterer, Mari Lahnalampi, Minna Voutilainen, Alexandra Brand, Gaia Gentile, Gabriele Greve, Bertram Bengsch, Merja Heinäniemi, Jesús Duque-Afonso involved in data analysis. Mira Kusterer, Mari Lahnalampi, Minna Voutilainen, Alexandra Brand, Merja Heinäniemi, and Jesús Duque-Afonso involved in manuscript drafting. Mira Kusterer, Mari Lahnalampi, Minna Voutilainen, Alexandra Brand, Michael Lübbert, Bertram Bengsch, Martin Werner, Justus Duyster, Olli Lohi, Merja Heinäniemi, Jesús Duque-Afonso involved in data interpretation and manuscript review for intellectual content. All authors involved in final approval for submission.

CONFLICT OF INTEREST STATEMENT

The authors declare no conflicting financial interest with the submission of this article. Jesús Duque-Afonso received speakers honoraria from Roche, Amgen, Riemser, SOBI, IPSEN, Abbvie, Beigene, NovoNordisk, and AstraZeneca and travel support from Lilly, Roche, Gilead, IPSEN, SOBI, and Beigene.

DATA AVAILABILITY STATEMENT

The data that support the findings of this study are openly available in Gene Expression Omnibus at https://www.ncbi.nlm.nih.gov/geo/, reference number GSE233937. The data generated during and/or analyzed during the current study are available upon reasonable request from the corresponding author. Processed data from genomics assays are available in Gene Expression Omnibus. Bulk data for RNAseq in the vehicle-treated mice are available in GEO GSE233937 and scRNAseq in GSE233940. CyTOF data were uploaded to FlowRepository after clean-up gating and debarcoding to single files. Title: Dynamic evolution of TCF3-PBX1 leukemias at the single-cell level under chemotherapy pressure. ID: FR-FCM-Z6K9.

ORCID

Emma Kaartinen http://orcid.org/0000-0001-9562-4366
Jesús Duque-Afonso https://orcid.org/0000-0002-8287-5673

SUPPORTING INFORMATION

Additional supporting information can be found in the online version of this article.

REFERENCES

1. Inaba H, Mullighan CG. Pediatric acute lymphoblastic leukemia. *Haematologica*. 2020;105:2524-2539. doi:10.3324/haematol.2020.247031
2. Jeha S, Pei D, Choi J, et al. Improved CNS control of childhood acute lymphoblastic leukemia without cranial irradiation: St Jude Total Therapy Study 16. *J Clin Oncol*. 2019;37:3377-3391. doi:10.1200/JCO.19.01692
3. Locatelli F, Zugmaier G, Rizzari C, et al. Effect of blinatumomab vs chemotherapy on event-free survival among children with high-risk first-relapse B-cell acute lymphoblastic leukemia: a randomized clinical trial. *JAMA*. 2021;325:843-854. doi:10.1001/jama.2021.0987
4. O'Brien MM, Ji L, Shah NN, et al. Phase II trial of inotuzumab ozogamicin in children and adolescents with relapsed or refractory B-cell acute lymphoblastic leukemia: Children's Oncology Group Protocol AALL1621. *J Clin Oncol*. 2022;40:956-967. doi:10.1200/JCO.21.01693
5. Myers RM, Li Y, Barz Leahy A, et al. Humanized CD19-targeted chimeric antigen receptor (CAR) T cells in CAR-naive and CAR-exposed children and young adults with relapsed or refractory acute lymphoblastic leukemia. *J Clin Oncol*. 2021;39:3044-3055. doi:10.1200/JCO.20.03458
6. Burmeister T, Gokbuget N, Schwartz S, et al. Clinical features and prognostic implications of TCF3-PBX1 and ETV6-RUNX1 in adult acute lymphoblastic leukemia. *Haematologica*. 2010;95:241-246. doi:10.3324/haematol.2009.011346
7. Barber KE, Harrison CJ, Broadfield ZJ, et al. Molecular cytogenetic characterization of TCF3 (E2A)/19p13.3 rearrangements in B-cell precursor acute lymphoblastic leukemia. *Genes Chromosomes Cancer*. 2007;46:478-486. doi:10.1002/gcc.20431
8. Jeha S, Pei D, Raimondi SC, et al. Increased risk for CNS relapse in pre-B cell leukemia with the t(1;19)/TCF3-PBX1. *Leukemia*. 2009;23:1406-1409. doi:10.1038/leu.2009.42
9. Krause S, Pfeiffer C, Strube S, et al. Mer tyrosine kinase promotes the survival of t(1;19)-positive acute lymphoblastic leukemia (ALL) in the central nervous system (CNS). *Blood*. 2015;125:820-830. doi:10.1182/blood-2014-06-583062
10. Duque-Afonso J, Feng J, Scherer F, et al. Comparative genomics reveals multistep pathogenesis of E2A-PBX1 acute lymphoblastic leukemia. *J Clin Invest*. 2015;125:3667-3680. doi:10.1172/JCI81158
11. Duque-Afonso J, Lin CH, Han K, et al. E2A-PBX1 remodels oncogenic signaling networks in B-cell precursor acute lymphoid leukemia. *Cancer Res*. 2016;76:6937-6949. doi:10.1158/0008-5472.CAN-16-1899
12. Lenk L, Carlet M, Vogiatzi F, et al. CD79a promotes CNS-infiltration and leukemia engraftment in pediatric B-cell precursor acute lymphoblastic leukemia. *Commun Biol*. 2021;4:73. doi:10.1038/s42003-020-01591-z
13. Lenk L, Winterberg D, Vogiatzi F, et al. Preclinical evidence for the efficacy of CD79b immunotherapy in B-cell precursor acute lymphoblastic leukemia. *HemaSphere*. 2022;6:e754. doi:10.1097/HS9.0000000000000754
14. Holleman A, Cheok MH, den Boer ML, et al. Gene-expression patterns in drug-resistant acute lymphoblastic leukemia cells and response to treatment. *N Engl J Med*. 2004;351:533-542. doi:10.1056/NEJMoa033513
15. Oshima K, Zhao J, Pérez-Durán P, et al. Mutational and functional genetics mapping of chemotherapy resistance mechanisms in relapsed acute lymphoblastic leukemia. *Nat Cancer*. 2020;1:1113-1127. doi:10.1038/s43018-020-00124-1

16. Holmfeldt L, Wei L, Diaz-Flores E, et al. The genomic landscape of hypodiploid acute lymphoblastic leukemia. *Nat Genet*. 2013;45:242-252. doi:10.1038/ng.2532

17. Paulsson K, Lilljebjörn H, Biloglav A, et al. The genomic landscape of high hyperdiploid childhood acute lymphoblastic leukemia. *Nat Genet*. 2015;47:672-676. doi:10.1038/ng.3301

18. Gu Z, Churchman ML, Roberts KG, et al. PAX5-driven subtypes of B-progenitor acute lymphoblastic leukemia. *Nat Genet*. 2019;51: 296-307. doi:10.1038/s41588-018-0315-5

19. Schroeder MP, Bastian L, Eckert C, et al. Integrated analysis of relapsed B-cell precursor Acute Lymphoblastic Leukemia identifies subtype-specific cytokine and metabolic signatures. *Sci Rep*. 2019;9: 4188. doi:10.1038/s41598-019-40786-1

20. Rabilloud T, Potier D, Pankaew S, Nozais M, Loosveld M, Payet-Bornet D. Single-cell profiling identifies pre-existing CD19-negative subclones in a B-ALL patient with CD19-negative relapse after CAR-T therapy. *Nat Commun*. 2021;12:865. doi:10.1038/s41467-021-21168-6

21. Good Z, Sarno J, Jager A, et al. Single-cell developmental classification of B cell precursor acute lymphoblastic leukemia at diagnosis reveals predictors of relapse. *Nat Med*. 2018;24:474-483. doi:10.1038/nm.4505

22. Mehtonen J, Teppo S, Lahnalampi M, et al. Single cell characterization of B-lymphoid differentiation and leukemic cell states during chemotherapy in ETV6-RUNX1-positive pediatric leukemia identifies drug-targetable transcription factor activities. *Genome Med*. 2020; 12:99. doi:10.1186/s13073-020-00799-2

23. Chen EY, Tan CM, Kou Y, et al. Enrichr: interactive and collaborative HTML5 gene list enrichment analysis tool. *BMC Bioinformatics*. 2013;14:128. doi:10.1186/1471-2105-14-128

24. Barsch M, Salié H, Schlaak AE, et al. T-cell exhaustion and residency dynamics inform clinical outcomes in hepatocellular carcinoma. *J Hepatol*. 2022;77:397-409. doi:10.1016/j.jhep.2022.02.032

25. Bradner JE, Hnisz D, Young RA. Transcriptional addiction in cancer. *Cell*. 2017;168:629-643. doi:10.1016/j.cell.2016.12.013

26. Ott CJ, Kopp N, Bird L, et al. BET bromodomain inhibition targets both c-Myc and IL7R in high-risk acute lymphoblastic leukemia. *Blood*. 2012;120:2843-2852. doi:10.1182/blood-2012-02-413021

27. Bliss CI. The calculation of microbial assays. *Bacteriol Rev*. 1956;20: 243-258. doi:10.1128/br.20.4.243-258.1956

28. Martín-Lorenzo A, Hauer J, Vicente-Dueñas C, et al. Infection exposure is a causal factor in B-cell precursor acute lymphoblastic leukemia as a result of Pax5-inherited susceptibility. *Cancer Discovery*. 2015;5:1328-1343. doi:10.1158/2159-8290.CD-15-0892

29. Baran-Marszak F, Boukhiar M, Harel S, et al. Constitutive and B-cell receptor-induced activation of STAT3 are important signaling pathways targeted by bortezomib in leukemic mantle cell lymphoma. *Haematologica*. 2010;95:1865-1872. doi:10.3324/haematol.2009.019745

30. Grüninger PK, Uhl F, Herzog H, et al. Functional characterization of the PI3K/AKT/MTOR signaling pathway for targeted therapy in B-precursor acute lymphoblastic leukemia. *Cancer Gene Ther*. 2022; 29:1751-1760. doi:10.1038/s41417-022-00491-0

31. Mostufi-Zadeh-Haghighi G, Veratti P, Zodel K, et al. Functional characterization of transforming growth factor-β signaling in dasatinib resistance and pre-BCR+ acute lymphoblastic leukemia. *Cancers*. 2023;15:4328. doi:10.3390/cancers15174328

32. Gambardella G, Viscido G, Tumaini B, Isacchi A, Bosotti R, di Bernardo D. A single-cell analysis of breast cancer cell lines to study tumour heterogeneity and drug response. *Nat Commun*. 2022;13:1714. doi:10.1038/s41467-022-29358-6

33. Su Y, Ko ME, Cheng H, et al. Multi-omic single-cell snapshots reveal multiple independent trajectories to drug tolerance in a melanoma cell line. *Nat Commun*. 2020;11:2345. doi:10.1038/s41467-020-15956-9

34. Aissa AF, Islam ABMMK, Ariss MM, et al. Single-cell transcriptional changes associated with drug tolerance and response to combination therapies in cancer. *Nat Commun*. 2021;12:1628. doi:10.1038/s41467-021-21884-z

35. Day C-P, Merlino G, Van Dyke T. Preclinical mouse cancer models: a maze of opportunities and challenges. *Cell*. 2015;163:39-53. doi:10.1016/j.cell.2015.08.068

36. Williams MTS, Yousafzai YM, Elder A, et al. The ability to cross the blood-cerebrospinal fluid barrier is a generic property of acute lymphoblastic leukemia blasts. *Blood*. 2016;127:1998-2006. doi:10.1182/blood-2015-08-665034

37. Savino AM, Fernandes SI, Olivares O, et al. Metabolic adaptation of acute lymphoblastic leukemia to the central nervous system microenvironment depends on stearoyl-CoA desaturase. *Nat Cancer*. 2020;1:998-1009. doi:10.1038/s43018-020-00115-2

38. Anderson D, Skut P, Hughes AM, et al. The bone marrow microenvironment of pre-B acute lymphoblastic leukemia at single-cell resolution. *Sci Rep*. 2020;10:19173. doi:10.1038/s41598-020-76157-4

39. Ebinger S, Özdemir EZ, Ziegenhain C, et al. Characterization of rare, dormant, and therapy-resistant cells in acute lymphoblastic leukemia. *Cancer Cell*. 2016;30:849-862. doi:10.1016/j.ccell.2016.11.002

40. Mallampati S, Leng X, Ma H, et al. Tyrosine kinase inhibitors induce mesenchymal stem cell-mediated resistance in BCR-ABL+ acute lymphoblastic leukemia. *Blood*. 2015;125:2968-2973. doi:10.1182/blood-2014-05-576421

41. Fernández-Sevilla LM, Valencia J, Flores-Villalobos MA, et al. The choroid plexus stroma constitutes a sanctuary for paediatric B-cell precursor acute lymphoblastic leukaemia in the central nervous system. *J Pathol*. 2020;252:189-200. doi:10.1002/path.5510

42. Jonart LM, Ebadi M, Basile P, Johnson K, Makori J, Gordon PM. Disrupting the leukemia niche in the central nervous system attenuates leukemia chemoresistance. *Haematologica*. 2020;105:2130-2140. doi:10.3324/haematol.2019.230334

43. Gaynes JS, Jonart LM, Zamora EA, Naumann JA, Gossai NP, Gordon PM. The central nervous system microenvironment influences the leukemia transcriptome and enhances leukemia chemoresistance. *Haematologica*. 2017;102:e136-e139. doi:10.3324/haematol.2016.152926

44. Kato I, Nishinaka Y, Nakamura M, et al. Hypoxic adaptation of leukemic cells infiltrating the CNS affords a therapeutic strategy targeting VEGFA. *Blood*. 2017;129:3126-3129. doi:10.1182/blood-2016-06-721712

45. Alsadeq A, Fedders H, Vokuhl C, et al. The role of ZAP70 kinase in acute lymphoblastic leukemia infiltration into the central nervous system. *Haematologica*. 2017;102:346-355. doi:10.3324/haematol.2016.147744

46. Alsadeq A, Lenk L, Vadakumchery A, et al. IL7R is associated with CNS infiltration and relapse in pediatric B-cell precursor acute lymphoblastic leukemia. *Blood*. 2018;132:1614-1617. doi:10.1182/blood-2018-04-844209

47. Cario G, Izraeli S, Teichert A, et al. High interleukin-15 expression characterizes childhood acute lymphoblastic leukemia with involvement of the CNS. *J Clin Oncol*. 2007;25:4813-4820. doi:10.1200/JCO.2007.11.8166

48. Irving J, Matheson E, Minto L, et al. Ras pathway mutations are prevalent in relapsed childhood acute lymphoblastic leukemia and confer sensitivity to MEK inhibition. *Blood*. 2014;124:3420-3430. doi:10.1182/blood-2014-04-531871

49. Gentile G, Poggio T, Catalano A, et al. Development of combination therapies with BTK inhibitors and dasatinib to treat CNS-infiltrating E2A-PBX1+/preBCR+ ALL. *Blood Adv*. 2024;8:2846-2860. doi:10.1182/bloodadvances.2023011582

50. Chan LN, Murakami MA, Robinson ME, et al. Signalling input from divergent pathways subverts B cell transformation. *Nature*. 2020; 583:845-851. doi:10.1038/s41586-020-2513-4

51. Abdelrasoul H, Vadakumchery A, Werner M, et al. Synergism between IL7R and CXCR4 drives BCR-ABL induced transformation in Philadelphia chromosome-positive acute lymphoblastic leukemia. *Nat Commun*. 2020;11:3194. doi:10.1038/s41467-020-16927-w

52. Geng H, Hurtz C, Lenz KB, et al. Self-enforcing feedback activation between BCL6 and pre-B cell receptor signaling defines a distinct subtype of acute lymphoblastic leukemia. *Cancer Cell*. 2015;27:409-425. doi:10.1016/j.ccell.2015.02.003

53. Messinger YH, Gaynon PS, Sposto R, et al. Bortezomib with chemotherapy is highly active in advanced B-precursor acute lymphoblastic leukemia: Therapeutic Advances in Childhood Leukemia & Lymphoma (TACL) Study. *Blood*. 2012;120:285-290. doi:10.1182/blood-2012-04-418640

54. Turati VA, Guerra-Assunção JA, Potter NE, et al. Chemotherapy induces canalization of cell state in childhood B-cell precursor acute lymphoblastic leukemia. *Nat Cancer*. 2021;2:835-852. doi:10.1038/s43018-021-00219-3

55. Dawson MA, Prinjha RK, Dittmann A, et al. Inhibition of BET recruitment to chromatin as an effective treatment for MLL-fusion leukaemia. *Nature*. 2011;478:529-533. doi:10.1038/nature10509

56. Fong CY, Gilan O, Lam EYN, et al. BET inhibitor resistance emerges from leukaemia stem cells. *Nature*. 2015;525:538-542. doi:10.1038/nature14888